Journal of Fluids and Structures 56 (2015) 1–10

Contents lists available at ScienceDirect

Journal of Fluids and Structures

journal homepage: www.elsevier.com/locate/jfs

Leaf flutter by torsional galloping: Experiments and model

Loïc Tadrist [a,b,*], Kévin Julio [a], Marc Saudreau [b], Emmanuel de Langre [a]

[a] École Polytechnique, Laboratoire d'hydrodynamique, 91128 Palaiseau, France
[b] INRA, Physique et Physiologie intégratives de l'arbre fruitier et forestier, 63100 Clermont-Ferrand, France

ARTICLE INFO

Article history:
Received 5 September 2014
Accepted 10 April 2015

Keywords:
Leaf
Flutter
Wind
Biomechanics
Aeroelastic instability

ABSTRACT

When wind blows on trees, leaves flutter. The induced motion is known to affect biological functions at the tree scale such as photosynthesis. This paper presents an experimental and theoretical study of the aeroelastic instability leading to leaf flutter. Experiments in a wind tunnel are conducted on ficus leaves (*Ficus Benjamina*) and artificial leaves. We show that stability and flutter domains are separated by a well-defined limit depending on leaf orientation and wind speed. This limit is also theoretically predicted through a stability analysis of the leaf motion.

© 2015 Elsevier Ltd. All rights reserved.

1. Introduction

Leaf motion of a tree is a common observation during a windy day. In fact, the Beaufort scale of wind intensity is based on the movement of leaves and branches: at Beaufort equal to 1, "leaves rustle", and then "leaves and twigs move", "small branches sway", "whole tree is in motion" at Beaufort levels of 3, 5 and 7 respectively. The Beaufort scale catches that the total leaf motion is the result of the combination of the global motion of the branch and the local motion of the leaf with respect to the branch it belongs to. In the general framework of flow-induced vibrations (Blevins, 1977; Naudascher, 1991; Païdoussis et al., 2010), it may be stated that the local leaf motion may result from forcing by wind turbulence, from coupling with the wake of the leaf, or from flutter. The present paper focuses on flutter, which is known to cause large increases of vibration amplitudes in short ranges of flow velocity (Grace, 1978).

Leaf flutter not only influences human perception of wind but also degrades radar or WIFI transmissions (Narayanan et al., 1994; Meng and Lee, 2010) and gives uncertainty on remote measurements of foliage characteristics (Kimes, 1984). More importantly, leaf flutter has many consequences, often beneficial, on key plant biological functions. It may reduce insect herbivory (Yamazaki, 2011) and enhance heat exchange (Schuepp, 1972; Grace, 1978), gas exchange (Nikora, 2010) and photosynthesis (Roden and Pearcy, 1993; Roden, 2003). The flutter of leaves may also be beneficial to reduce the water retention of the foliage and thereby to eject pathogens with the water droplets.

The mechanics of plant dynamics under wind have been studied in many aspects, see the review by de Langre (2008). Most of the existing work focuses on overall tree sway (Mayer, 1987; Kerzenmacher and Gardiner, 1998; Sellier and Fourcaud, 2005; Rodriguez et al., 2012) or crop canopy motion (Py et al., 2005, 2006; Dupont and Gosselin, 2010). At the leaf scale, wind is known to affect the time-averaged position of the leaf, as well as its shape, a mechanism generically referred to as reconfiguration (Vogel, 1989; Gosselin et al., 2010; Tadrist et al., 2014). In terms of leaf oscillation, Roden (2003) modeled the aspen leaf flutter as a given periodic rotation, and the work of Niklas (1991) could let us think that poplar leaf

* Corresponding author at: École polytechnique, Laboratoire d'hydrodynamique, 91128 Palaiseau, France. Tel.: +33 674100203.
E-mail address: loic.tadrist@ladhyx.polytechnique.fr (L. Tadrist).

http://dx.doi.org/10.1016/j.jfluidstructs.2015.04.001
0889-9746/© 2015 Elsevier Ltd. All rights reserved.

motion is probably a case of classical coupled mode flutter. Miller et al. (2012) have shown on tulip tree leaves that leaf reconfiguration reduces leaf vortex shedding and thus leaf vibration. Leaves of aquatic plants have also been studied (Puijalon et al., 2005; Miller et al., 2012), with similar conclusions. Yet, it has been pointed out by Pearcy (1990) and more recently Rascher and Nedbal (2006) that little is known about the mechanical processes resulting in leaf motion under wind.

The goal of the present investigation is to study and describe the mechanics of leaf flutter using both experimental and theoretical approaches. To do so, we explore the influence of wind velocity and leaf parameters, mechanical or geometrical, on the existence of leaf flutter.

In Section 2 we show that leaf flutter is actually torsional galloping, using ficus leaves (*Ficus Benjamina*) in a wind tunnel. In Section 3, using artificial leaves, we explore more systematically the effects of mechanical and geometrical parameters on the existence of flutter. With the help of standard concepts of aeroelasticity, a model is proposed in Section 4, and compared with the experiments. A discussion of mechanical and biological issues is given in Section 5.

2. Experiments on real leaves

2.1. Evidence of torsional flutter

As a first step we test ficus leaves (*Ficus Benjamina*), such as illustrated in Fig. 1a. Leaves are taken from a tree using standard practices in plant biomechanics in order to preserve their mechanical properties. Individual leaves are inserted in a wind tunnel, as in Tadrist et al. (2014), and their bending and torsional deformation are measured optically, as a function of the wind velocity, U. Leaves are held by pliers and their inclination angle may be varied by a wheel, see Fig. 1b.

To illustrate the generic behavior of those leaves under wind, we show in Fig. 2a a typical evolution of the bending angle, δ, and the torsion angle amplitude, $\Delta\theta$, with the wind velocity. The wind load on the lamina (the flat part of the leaf) results in bending of the petiole (the beam-like connection between the branch and the lamina). The static deformation

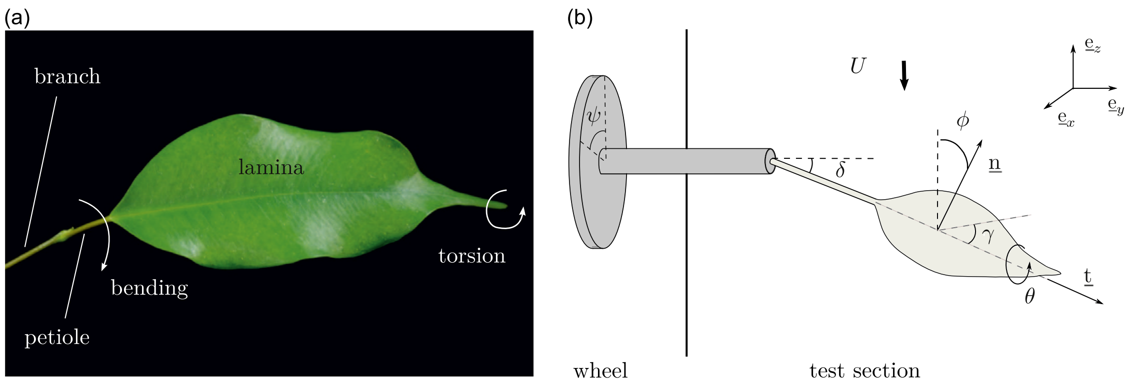

Fig. 1. (a) Leaf components and motion. (b) Schematic view of the set-up and definition of angles used to define the position of the leaf.

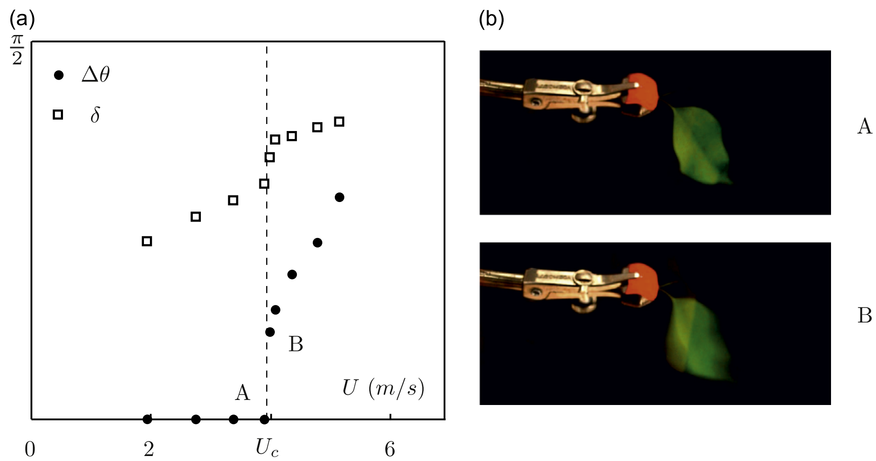

Fig. 2. Deformation and flutter of a ficus leaf. (a) Evolution of the bending angle, δ, (square) and of the amplitude of torsional motion, $\Delta\theta$, (●) showing the onset of flutter, U_c. (b) View of the leaf below and above the onset of flutter, points A and B in (a).

Table 1
Nomenclature.

l	Lamina length
w	Lamina width
A	Leaf area
p	Leaf perimeter
P	Palmation index
β	Petiole insertion angle
Λ	Center of gravity to petiole end distance
J	Moment of inertia in torsion
f_0	Leaf torsional eigen frequency
ω_0	Leaf torsional eigen pulsation
ξ	Leaf torsional damping
M_f	Moment of the fluid on the leaf
U	Wind velocity
ρ	Air density
C_M	Aerodynamic moment coefficient
ψ	Wheel support rotation angle
δ	Angle between branch and petiole
ϕ	Angle between lamina normal vector and wind direction
θ	Angle of torsion of the lamina along its axis
α	Angle between wind direction and lamina normal vector, in the lamina reference frame
γ	Projection angle of moment
$\mathcal{M}$	Mass number
U_r	Reduced velocity

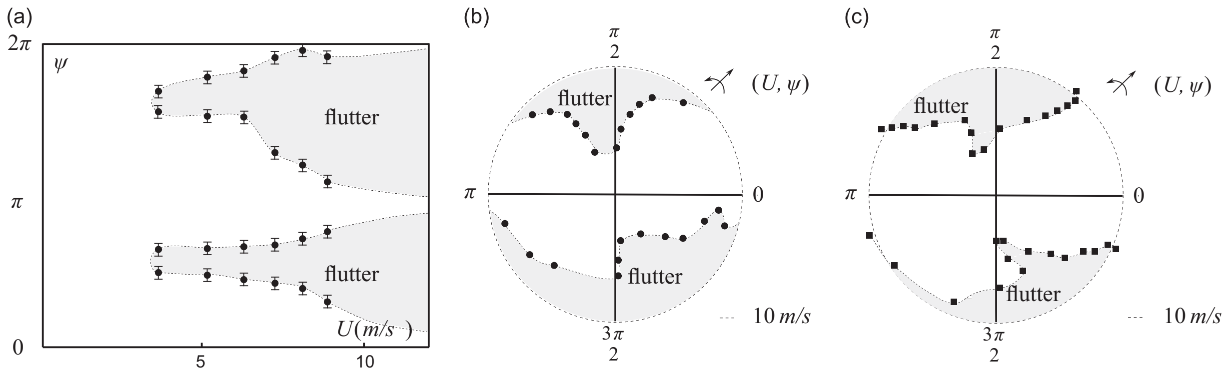

Fig. 3. (a) Zone of flutter of the Ficus leaf 1 in the space of wind speed and inclination angle. At the border, the leaf starts to vibrate in torsion. (b) Same results, in polar coordinate (U, ψ). (c) Same test for Ficus leaf 2.

corresponds to reconfiguration effects as aforementioned. Note that the wind-induced change of the bending angle is here close to $\pi/2$. Simultaneously, the torsion angle of the lamina along its main axis evolves as follows: for lower wind velocities, up to 4 m/s here, no motion is observed. Above this velocity the leaf flutters in torsion, with an amplitude that increases suddenly with U, reaching about $\pi/4$ at 5 m/s. The flutter observed here, in pure torsion, will also be referred to as torsional galloping in the following, anticipating Section 4 where a model is proposed. For higher velocities, more complex motions are observed combining several degrees of freedom of the leaf dynamics (Table 1).

2.2. Domain of torsional galloping

We focus now on the critical value of the wind velocity U_c that corresponds to the onset of torsional galloping, $U_c = 4$ m/s in Fig. 2. Experimentally, for a given wind velocity, U, we vary the angle ψ of the clamped end, Fig. 1b, to explore the range of torsional galloping. An angle ψ=0 corresponds to the lamina plane being perpendicular to the flow velocity when there is no flow-induced bending. In the same manner, an angle $\psi = \pi/2$ corresponds to the flow being tangential to the lamina plane. The domain of flutter for a leaf is given in the (U, ψ) parameters space, Fig. 3a. The error bar in ψ corresponds to a small hysteresis effect observed when the sign of variation of ψ is changed. This small effect is discarded in the following. Fig. 3a shows that torsional flutter is observed for all angles between the leaf and the wind axis, except for ψ=0 and π, where the leaf is set perpendicular to the flow. For the sake of clarity, the same results are also presented in a common polar plot using (U, ψ) variables, see Fig. 3b. The asymmetry between upper and lower stability regions results from non-

Table 2
Numerical values of leaves parameters.

	A (cm^2)	w (cm)	l (cm)	Λ (cm)	p (cm)	β (–)	δ (–)	J (10^{-7} kg m^2)	f_0 (Hz)	ξ (%)	Symbol
Ficus leaf 1	12.4	2.8	7.1	3.6	19.6	$\pi/6$	0	0.27	14.1	5.2	●
Ficus leaf 2	10.0	3.2	7	3.6	20.4	$\pi/6$	0	0.55	8.4	7.8	■
Artificial leaf (A)	23.8	5.5	5.5	2.8	17.3	0	0	4.7	12.3	1.7	○
Artificial leaf (B)	23.8	5.5	5.5	2.8	17.3	$\pi/4$	0	4.7	4.01	2.7	△
Artificial leaf (C)	23.8	5.5	5.5	2.8	17.3	0	$\pi/3$	4.7	3.87	2.7	★
Artificial leaf (D)	16.3	5	6.2	2.3	25	0	0	5.2	7.9	3.1	□

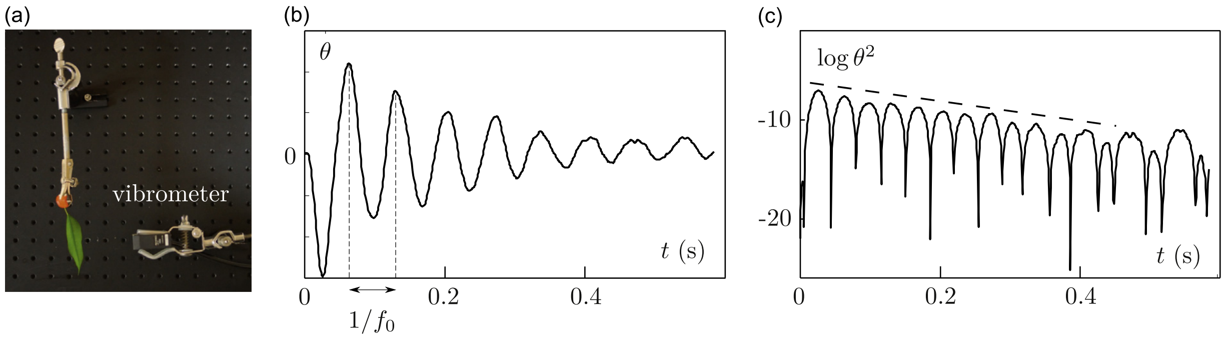

Fig. 4. Torsion mode of a leaf. (a) Experimental set-up. (b) and (c) Time evolution of the torsion angle.

symmetric values of geometrical and mechanical parameters between the upper and the lower side of the leaf. To exemplify the effect of variability among leaves, the stability domain of another leaf from the same ficus tree is shown in Fig. 3c. A similar behavior is observed although the two leaves differ in many aspects (size, shape, mass, etc.), see Table 2.

These experiments on real leaves show that the angle of inclination of the leaf towards the wind has a crucial impact on torsional galloping.

Considering that flutter occurs essentially in torsion along the leaf axis, the frequency and damping of the torsion mode in still air are measured. This is done on the leaves clamped as above but the torsion motion being now measured through a laser sensor (*micro-epsilon ILD1300-20*). The leaf is excited manually and the free motion is recorded. The frequency, f_0, and damping coefficient, ξ, are derived using basic fitting technique (Bert, 1973). This procedure is illustrated in Fig. 4. The moment of inertia in torsion, J, is estimated through weighting of the leaf and using $J = mw^2/12$ where m is the mass and w is the width of the leaf. The results are given in Table 2 for the two ficus leaves.

We now turn to artificial leaves where geometrical and mechanical parameters can be controlled.

3. Experiments on artificial leaves

3.1. Geometrical parameters

We give in Fig. 5, the geometrical parameters used hereafter to discuss the geometry of a leaf in the following. First, the shape of the lamina is defined by five parameters: the area, A, the width and the height, w and l, the distance from base to center of mass, Λ, and the perimeter, p. Two angles need also to be defined, that between the lamina and the petiole, β, and that of insertion between the petiole and the branch, δ, Fig. 5. Typical values of these parameters are given in Table 2 for the ficus leaves used in the preceding section. We may define the following dimensionless parameters, A/wl, w/l, Λ/l and the palmation index $P = 2\sqrt{\pi A}/p$ which scales the complexity of the shape of the leaf perimeter (P=1 for a circular shape).

Four different artificial leaves are now used, which allow us to test the influence of these dimensionless parameters, Fig. 5b. Leaf A is a simple disk, with both angles β and δ set to zero. Leaf B has the same shape but with an angle between lamina and petiole, $\beta = \pi/4$ and δ=0. Conversely, in leaf C, β=0 and $\delta = \pi/3$. To define, leaf D, we rely on the data base LEAF (2010) which gives about 90 shapes of lamina of simple leaves from typical European forest tree species. Some of the shapes are illustrated in Fig. 6a. The four dimensionless parameters defined above are computed on all the species and displayed in terms of probability density functions, see Fig. 6b. This allows us to define an *average* leaf which has a shape corresponding to the average values of all parameters. This average leaf is not uniquely defined; we give in Fig. 5b the shape used hereafter, named leaf D, which satisfies these conditions, namely $A/wl = 0.54$, $w/l = 0.61$, $\Lambda/l = 0.43$ and P=0.57. The dimensional and dimensionless geometrical parameters of all leaves are given in Tables 2 and 3 respectively.

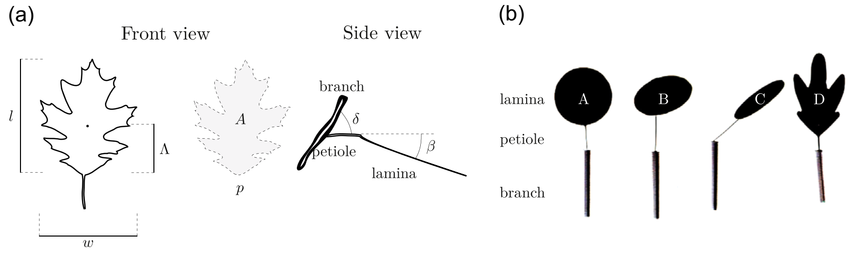

Fig. 5. (a) Geometrical parameters used to describe the leaf. (b) Artificial leaves used in the experiment.

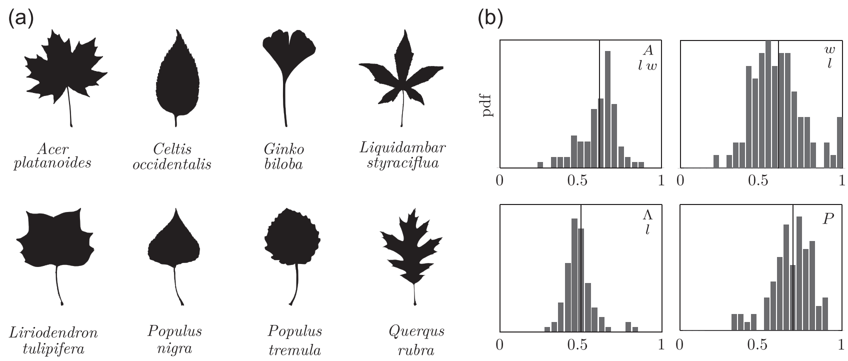

Fig. 6. (a) Typical shapes of leaves from the data base LEAF (2010). (b) Probability density functions of the dimensionless geometrical parameters considering all species of the database. The average values satisfied by leaf D are shown by a vertical line.

Table 3
Dimensionless geometrical and mechanical parameters for the leaves used in the experiment.

	A/wl	w/l	Λ/l	P	β	δ	$\mathcal{M}$	ξ
Ficus leaf 1	0.62	0.39	0.50	0.63	$\pi/6$	0	0.15	5.2
Ficus leaf 2	0.43	0.45	0.51	0.55	$\pi/6$	0	0.09	7.8
Artificial leaf (A)	$\pi/4$	1	0.5	1	0	0	0.10	1.7
Artificial leaf (B)	$\pi/4$	1	0.5	1	$\pi/4$	0	0.10	2.7
Artificial leaf (C)	$\pi/4$	1	0.5	1	0	$\pi/3$	0.10	2.7
Artificial leaf (D)	0.53	0.61	0.43	0.57	0	0	0.05	3.1

3.2. Galloping of artificial leaves

The four lamina shapes (A, B, C, and D), in rigid plastic, are mounted on flexible petioles made of piano wires. The mechanical parameters of these artificial leaves are obtained using the same procedure as for the ficus leaves, see Section 2.2. The moment of inertia in torsion is computed with the actual shape of each leaf. The corresponding values of f_0, ξ and J are given in Table 2. These artificial leaves are inserted in the wind tunnel and their behavior is explored, for increasing flow velocity, varying also the wheel angle ψ.

As for the ficus leaves, we observe a sudden transition to torsional flutter when the wind velocity is increased, strongly dependent on the orientation angle ψ. The flutter domain in (U,ψ) parameters of the four leaves is given in Fig. 7. Note that leaves A and D being up/down and right/left symmetric, only one quadrant was explored. The shapes of the flutter domains are generally similar with some differences in leaves B and C. The magnitude of the flow velocity at the onset of flutter depends on the leaf parameters. Note that for leaf C, near $\psi=\pi$, a zone of flutter involving a completely different motion was observed. This seems to be due to a very high bending curvature of the petiole in that position.

These same experimental results are now rescaled using standard dimensionless parameters in aeroelasticity (Blevins, 1977; Larsen, 2002; Robertson et al., 2003; Païdoussis et al., 2010), namely the mass number $\mathcal{M}$, the reduced velocity U_R and the damping ratio ξ, combined in $\mathcal{M}U_R/\xi$. We define the former as

$$\mathcal{M}=\frac{\rho A w^3}{8J} \quad \text{and} \quad U_R=\frac{U}{f_0 w}. \tag{1}$$

The values of $\mathcal{M}$ and ξ for each leaf are found in Table 3. Fig. 7 shows the flutter boundary for all artificial leaves, in the ($\mathcal{M}U_R/\xi$,ψ) space. The behavior of all four artificial leaves seems qualitatively similar and much more dependent on ψ than

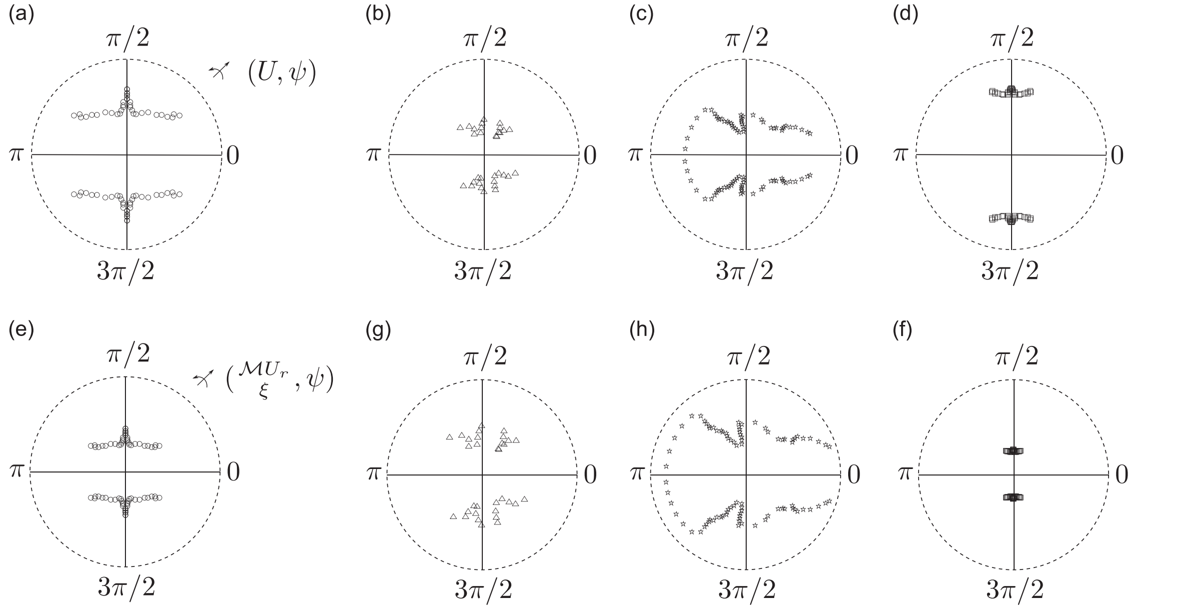

Fig. 7. Limits of torsional flutter of leaves A, B, C and D. Labels (a)–(d) refer to a representation in (U,ψ) space and (e)–(h) to $(\mathcal{M}U_r/\xi,\psi)$ space. The outer circles correspond to $U=15$ m/s and $\mathcal{M}U_r/\xi=80\pi$.

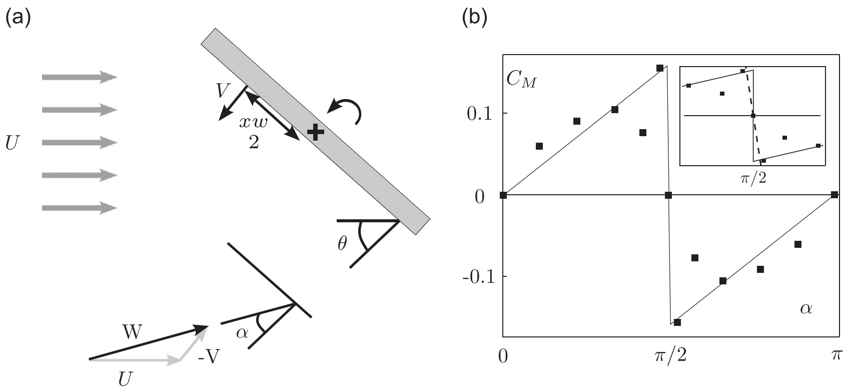

Fig. 8. (a) Schematic view of the change of angle towards the rotating surface. The distance $xw/2$ allows us to determine the reference speed on the plate and the reference angle α. (b) Evolution of moment coefficient C_M as a function of the incident angle α, from experimental values of Wick (1954). Between $\pi/2$ and π, the graph is built by symmetry (■) experiments (–) model. Inset shows an enlargement of the curve close to $\pi/2$ where lifting line theory applies. Dashed line (- -) represents the lifting line theory, $C_M(\alpha)=\pi/2(\pi/2-\alpha)$.

all other geometrical parameters. This conclusion naturally leads to explore the possibility of a simple model of torsional galloping to account for the dynamics of leaves under wind.

4. Model for leaf flutter

4.1. Aeroelastic model

In the framework of a plane leaf lamina in a flow, several angles have to be defined to describe the flow loading. Using $\underline{n}$, the normal to the lamina, and $\underline{t}$, the axis of rotation of the lamina, we define $\phi=\langle\underline{n},\underline{U}\rangle$ and $\gamma=\langle\underline{n}\times\underline{U},\underline{t}\rangle$, see Fig. 1b. They depend on the other angles β, δ and ψ defined above by $\cos\phi=\cos(\delta+\beta)\cos\psi$ and $\cos\gamma=\sin\psi/\sin\phi$.

Let M be the moment of the aerodynamic load on the $\underline{t}$ axis. To model torsional flutter observed in the experiments we use the simplest linear quasi-steady approach of torsional galloping (Blevins, 1977; Larsen, 2002; Païdoussis et al., 2010; Fernandes and Armandei, 2014; Armandei and Fernandes, 2014) whereby the torsion moment depends on a reference angle of attack, α, which itself depends on a reference relative velocity. Note that this approach is known to be unable to capture several aspects of torsional galloping, see the discussion in Païdoussis et al. (2010); we nevertheless use it here as a first approximation of the phenomenon. In the general geometrical case, taking into account all the angles above leads to rather complex equations: we give here the equations for the simple case $\delta=0$, $\beta=0$, where $\gamma=0$ and $\phi=\psi$. The general case is

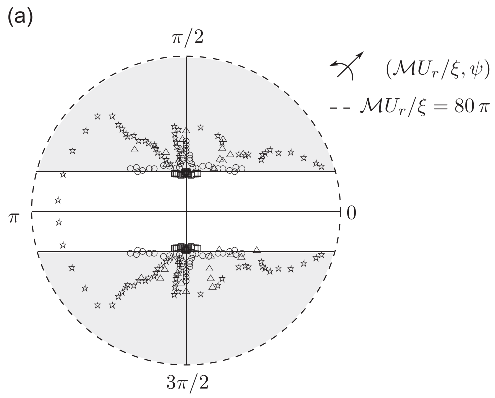

Fig. 9. Limits of torsional galloping predicted by the model and comparison with experimental data (a) for artificial leaves A, B, C and D and (b) for ficus leaves 1 and 2. The shaded area correspond to flutter according to the model.

given in Appendix A. In that simpler case, the variations of the moment of torsion, for a small variation of the angle $\theta(t)$ may be approximated by

$$M = \frac{1}{4}\rho U^2 A w \frac{\partial C_M}{\partial \alpha}\frac{\partial \alpha}{\partial \dot{\theta}}\dot{\theta}, \tag{2}$$

where $C_M(\alpha)$ is the moment coefficient, $\dot{\theta}$ is the time derivative of θ, the area A and width w having been defined before. Note that stiffness terms, proportional to θ, are not included in Eq. (2) for the sake of clarity. The reference angle of attack is defined here by

$$\alpha = \psi + x\frac{w\dot{\theta}}{2U}\sin\psi, \tag{3}$$

where x defines the position of the point where the solid velocity has been taken to define α ($x=1$ is the leading edge and $x=0$ is the mid-chord), Fig. 8a.

The dynamic stability of the torsion mode is classically derived comparing the flow damping to the internal damping in the equation of motion

$$J\ddot{\theta} + 2J\xi\omega\dot{\theta} + J\omega^2\theta = M. \tag{4}$$

This reads, in dimensionless form,

$$\ddot{\theta} + \left(2\xi - \frac{x}{2\pi}\mathcal{M}U_R\frac{\partial C_M}{\partial \alpha}\sin\psi\right)\dot{\theta} + \theta = 0, \tag{5}$$

and torsion galloping is expected to occur when damping vanishes, or

$$U_R > \frac{4\pi\xi}{\mathcal{M}}\frac{1}{\sin\psi}\frac{1}{(x\partial C_M/\partial\alpha)} \quad \text{or equivalently}$$
$$\left(x\frac{\partial C_M}{\partial \alpha}\right)\frac{\mathcal{M}U_R}{\xi}\sin\psi > 4\pi. \tag{6}$$

In the most general case, $\delta \neq 0$ and $\beta \neq 0$, elementary geometrical considerations actually lead to the same results, see Appendix A. The key elements of this type of model are the position of the reference velocity, x, and the moment coefficient $C_M(\alpha)$ through the product $x\partial C_M/\partial\alpha$. Little is known on these two parameters for the complex shapes of leaves or even for the disk used here.

4.2. Comparison with experiments

If we assume that x and $\partial C_M/\partial\alpha$ do not vary much with the angle of incidence, then so does not the product, and the flutter condition, Eq. (6), reads

$$\frac{\mathcal{M}U_R}{\xi}\sin\psi > C, \tag{7}$$

where $C = 4\pi/(x\partial C_M/\partial\alpha)$ is a constant. In polar representation, in the $(\mathcal{M}U_R/\xi, \psi)$ space, the flutter domain is thus bounded by two straight horizontal lines. By fitting such horizontal lines on the experimental data, Fig. 9, we have $C = 20\pi$, corresponding to $x\partial C_M/\partial\alpha = 0.2$. This value is compatible with values for thin rectangular plates with x in the range 0.5–1, (Païdoussis et al., 2010, pp. 66–70) and $\partial C_M/\partial\alpha = 0.1$ (Wick, 1954, Fig. 8b), leading to $x\partial C_M/\partial\alpha = 0.05--0.1$.

The model does not capture the slightly increased stability observed in the experiments on artificial leaves, close to $\psi = \pi/2$ or $3\pi/2$, when the flow is tangential to the leaf. This is expected as the sign of $\partial C_M/\partial\alpha$ does actually change there, Fig. 8b, a feature not taken into account in our model.

5. Discussion

As emphasized in the previous sections, the geometrical and mechanical parameters of leaves are immensely varied among species, and even among the leaves of a single tree, see Fig. 6. Moreover, wind does change some of these parameters, the static bending and torsion of the petiole changing the angles and the effective torsion rigidity of the petiole and thereby the torsion frequency and mode shape. In fact, the criterion given in Eq. (7), expressed in terms of dimensional quantities, reads,

$$\frac{\rho}{m/A}\frac{U}{f_0\xi}\sin\psi > \frac{40\pi}{3}. \tag{8}$$

This shows that the angles δ and β may change by elastic deformation without direct influence on the limit of flutter. The indirect effect of deformation of the petiole on the frequency f_0 will just shift the critical velocity. Moreover only the mass per unit area (m/A) counts in Eq. (8), a quantity fairly independent of the size of the leaf lamina, at least in a given tree. Hence the size of the lamina only influences the critical velocity through the frequency, f_0, which depends on the total leaf mass. The palmation index of the leaf, P, and even its flatness seem not to influence the onset of torsional flutter as it can be seen from the behavior of leaf D or of the real leaves, when compared to the circular plane artificial leaves, see Fig. 9. Therefore, torsional galloping as described here seems a rather robust mechanism in terms of its dependency on geometrical and mechanical parameters.

In the experiments and the model, we have only considered the onset of flutter. Actually, we have observed that at higher velocities (20% higher than the critical velocity, 5 m/s for ficus leaves), complex motions of leaves arise, involving bending and torsion of extremely large amplitudes and irregular temporal evolution. These large motions do exist in nature, but the major transition is between no motion and torsional flutter, as most of the time a leaf experiences low wind velocities.

Translational galloping may arise if torsional galloping is prevented, for example by a strong anisotropy of the petiole or simply if the torsional stiffness is much higher than the bending stiffness. A case of pure translational galloping, near $\psi = 0$, has been observed for artificial leaves when the torsion mode was artificially canceled by a strong anisotropy of the petiole. Coupled mode flutter involving torsion and bending modes, as expected from Niklas (1991), was never observed here, probably because the frequencies in torsion and bending differed significantly. Both the model and ficus leaves exhibited a torsional motion at the onset of flutter. It seems likely that most leaves experience torsional motion, but more species need to be considered to confirm this.

In nature, a leaf is not made of a 2D lamina plane and an homogeneous and isotropic petiole. The lamina is more likely to be a 3D surface because of growth or reconfiguration. This may change the aerodynamic moment coefficient $C_M(\alpha)$ of the leaf and the critical wind speed as well as the angle at which the leaf starts to flutter. The anisotropy of the petiole may change the kinematics of galloping, as observed here when the artificial petiole was made strongly anisotropic.

We have explored here the flutter of a single leaf without any neighbor. On a tree, leaves may interact with each other by their wakes, by impacts, by leaf to leaf friction or by their folding into clusters (Vogel, 1989). Our model, which does not take into account interactions between leaves, is more adapted to trees with sparse foliage.

We may now discuss the potential use of these results in predicting the behavior of the whole foliage under wind. First, we may combine the criterion of Eq. (7) with the models of distribution of orientation of leaves in a tree (Tadrist et al., 2014). Assuming that all leaves are identical except for their orientation, we may predict numerically the proportion of the total leaf population that flutters at a given flow velocity, a quantity of interest for photosynthesis (Pearcy, 1990; Rascher and Nedbal, 2006). Using the distribution of leaf orientation of an idealized tree (Fig. 7 in Tadrist et al., 2014), the proportion of leaves that flutter is found to shift from 0 to 0.9 in a short range of velocities, $U/U_c = 1$ to 1.5, where U_c is the velocity where the first leaf flutters. This shows that foliage flutter is expected to appear as a sudden global phenomenon. The present approach may also be used to predict more complex quantities such as amplitudes and frequencies of flutter, which govern the ejection of rain drops or pesticides from the foliage (Carlson et al., 1976). Furthermore, the full motion of the foliage may be modeled by combining the deformation of the branched tree structure (Rodriguez et al., 2008) in response to the wind turbulence, and the present model of leaf flutter. As stated in the Beaufort scale mentioned at the beginning of the paper, we expect that as wind increases, leaves, twigs, small branches and then large branches are successively set into motion.

Acknowledgment

The authors gratefully acknowledge fruitful discussions with Bruno Moulia, Sara Puijalon, Xavier Amandolese and Pascal Hémon. They also thank Pascal Hémon for precious help building the experiment.

Appendix A

A.1. Geometrical relations between angles

The mid-chord direction of the leaf, $\underline{t}$, and normal vector, $\underline{n}$, read,

$$\underline{t} = \left| \begin{array}{l} -\sin\psi \sin(\delta+\beta) \\ \cos(\delta+\beta) \\ -\cos\psi \sin(\delta+\beta) \end{array} \right. \quad \text{and} \quad \underline{n} = \left| \begin{array}{l} \sin\psi \cos(\delta+\beta) \\ \sin(\delta+\beta) \\ \cos\psi \cos(\delta+\beta) \end{array} \right. . \tag{A.1}$$

We define the vector $\underline{q}$ as the normalized cross product of $\underline{n}$ and $\underline{e}_z$

$$\underline{q} = \frac{1}{\sin\phi}\underline{e}_z \times \underline{n} = \frac{1}{\sin\phi} \left| \begin{array}{l} -\sin(\delta+\beta) \\ \sin\psi\cos(\delta+\beta) \\ 0 \end{array} \right. . \tag{A.2}$$

Then by defining $\cos\phi = \underline{n}.\underline{e}_z$ and $\cos\gamma = \underline{q}.\underline{t}$, we have

$$\cos\phi = \cos\psi \cos(\delta+\beta) \quad \text{and} \quad \cos\gamma = \frac{\sin\psi}{\sin\phi}. \tag{A.3}$$

A.2. Derivation of the reference angle of incidence α

In the leaf reference frame, $\underline{V} = \underline{U} + xw\dot{\theta}\underline{n}/2$. Using Eqs. (A.1) and (A.3), we obtain, at the first order in $w\dot{\theta}/U$,

$$\frac{-\underline{V}\cdot\underline{n}}{|\underline{V}|} = \frac{(U\cos\psi\cos(\delta+\beta) - xw\dot{\theta}/2)}{\sqrt{U^2 - Uxw\dot{\theta}\cos\psi\cos(\delta+\beta)}} \tag{A.4}$$

$$\frac{-\underline{V}\cdot\underline{n}}{|\underline{V}|} \approx \frac{(U\cos\psi\cos(\delta+\beta) - xw\dot{\theta}/2)}{U(1 - xw\dot{\theta}/u\cos\psi\cos(\delta+\beta)/2)} \tag{A.5}$$

$$\frac{-\underline{V}\cdot\underline{n}}{|\underline{V}|} \approx \cos\psi\cos(\delta+\beta) + \frac{xw\dot{\theta}}{2U}\left(\cos^2\psi\cos^2(\delta+\beta) - 1\right). \tag{A.6}$$

By using the definition, $\alpha = \arccos(-\underline{V}\cdot\underline{n}/|\underline{V}|)$, we have

$$\alpha \approx \arccos\left(\cos\psi\cos(\delta+\beta)\right) + \frac{xw\dot{\theta}}{2U}\sqrt{1 - \cos^2\psi\cos^2(\delta+\beta)} = \phi + \frac{xw\dot{\theta}}{2U}\sin\phi. \tag{A.7}$$

In the simplified case, $\beta=0$ and $\delta=0$ leads to $\phi=\psi$ and thus

$$\alpha \approx \psi + \frac{xw\dot{\theta}}{2U}\sin\psi. \tag{A.8}$$

A.3. General model with $\beta \neq 0$ and $\delta \neq 0$

In that case, the coefficient of fluid moment is changed by a factor $\cos\gamma$ due to the angle between the torsion axis and the incidence of fluid on the plate

$$M = \frac{1}{4}\rho U^2 A w \frac{\partial C_M}{\partial\alpha}\frac{\cos\gamma\,\partial\alpha}{\partial\dot{\theta}}\dot{\theta}. \tag{A.9}$$

Using the full expression of α, Eq. (A.7), one can express the limit for torsional galloping

$$x\frac{\mathcal{M}U_R}{\xi}\frac{\partial C_M}{\partial\alpha}\cos\gamma\sin\phi > 4\pi. \tag{A.10}$$

Eventually, with Eq. (A.3), the final result is strictly the same as in the simplified case

$$x\frac{\mathcal{M}U_R}{\xi}\frac{\partial C_M}{\partial\alpha}\sin\psi > 4\pi. \tag{A.11}$$

References

Armandei, M., Fernandes, A., 2014. Torsional instability of an elastic flat plate due to hydrodynamic loads. Journal of Mechanics, 1–8.

Bert, C.W., 1973. Material damping: an introductory review of mathematic measures and experimental technique. Journal of Sound and Vibration 29, 129–153.

Blevins, R.D., 1977. Flow-induced Vibration, vol. 1. Van Nostrand Reinhold Co, New York.

Carlson, R.W., Bazzaz, F.A., Stukel, J.J., Wedding, J.B., 1976. Physiological effects, wind reentrainment, and rainwash of lead aerosol particulate deposited on plant leaves. Environmental Science & Technology 10, 1139–1142.

Dupont, S., Gosselin, F., Py, C., de Langre, E., Hemon, P., Brunet, Y., 2010. Modelling waving crops using large-eddy simulation: comparison with experiments and a linear stability analysis. Journal of Fluid Mechanics 652, 5–44.

Fernandes, A.C., Armandei, M., 2014. Phenomenological model for torsional galloping of an elastic flat plate due to hydrodynamic loads. Journal of Hydrodynamics, Series B 26, 57–65.

Gosselin, F., de Langre, E., Machado-Almeida, B.A., 2010. Drag reduction of flexible plates by reconfiguration. Journal of Fluid Mechanics 650, 319–341.

Grace, J., 1978. The turbulent boundary layer over a flapping populus leaf. Plant, Cell & Environment 1, 35–38.

Kerzenmacher, T., Gardiner, B., 1998. A mathematical model to describe the dynamic response of a spruce tree to the wind. Trees 12, 385–394.

Kimes, D., 1984. Modeling the directional reflectance from complete homogeneous vegetation canopies with various leaf-orientation distributions. Journal of Optical Society of America A 1, 725–737.

de Langre, E., 2008. Effects of wind on plants. Annual Review of Fluid Mechanics 40, 141–168.

Larsen, A., 2002. Torsion galloping of elongated bluff cross sections. In: ASME 2002 International Mechanical Engineering Congress and Exposition, vol. 1, pp. 403–409.

LEAF, 2010. Tree Leaf Database. Institute of Information Theory and Automation ASCR, Prague, Czech Republic. ⟨http://zoi.utia.cas.cz/tree_leaves⟩.

Mayer, H., 1987. Wind-induced tree sways. Trees 1, 195–206.

Meng, Y.S., Lee, Y.H., 2010. Investigations of foliage effect on modern wireless communication systems: a review. Progress in Electromagnetics Research 105, 313–332.

Miller, L.A., Santhanakrishnan, A., Jones, S., Hamlet, C., Mertens, K., Zhu, L., 2012. Reconfiguration and the reduction of vortex-induced vibrations in broad leaves. Journal of Experimental Biology 215, 2716–2727.

Narayanan, R., Doerr, D., Rundquist, D., 1994. Power spectrum of wind-influenced vegetation backscatter at x-band. IEE Proceedings—Radar, Sonar and Navigation 141, 125–131.

Naudascher, E., 1991. IAHR Hydraulic Structures Design Manual: Hydraulic Design Considerations. Hydrodynamic Forces. Balkema, Rotterdam, Netherlands.

Niklas, K.J., 1991. The elastic moduli and mechanics of populus tremuloides (salicaceae) petioles in bending and torsion. American Journal of Botany 78, 989–996.

Nikora, V., 2010. Hydrodynamics of aquatic ecosystems: an interface between ecology, biomechanics and environmental fluid mechanics. River Research and Applications 26, 367–384.

Païdoussis, M.P., Price, S.J., de Langre, E., 2010. Fluid–Structure Interactions: Cross-Flow-Induced Instabilities. Cambridge University Press, New York, USA.

Pearcy, R.W., 1990. Sunflecks and photosynthesis in plant canopies. Annual Review of Plant Biology 41, 421–453.

Puijalon, S., Bornette, G., Sagnes, P., 2005. Adaptations to increasing hydraulic stress: morphology, hydrodynamics and fitness of two higher aquatic plant species. Journal of Experimental Botany 56, 777–786.

Py, C., de Langre, E., Moulia, B., 2006. A frequency lock-in mechanism in the interaction between wind and crop canopies. Journal of Fluid Mechanics 568, 1–4.

Py, C., de Langre, E., Moulia, B., Hémon, P., 2005. Measurement of wind-induced motion of crop canopies from digital video images. Agricultural and Forest Meteorology 130, 223–236.

Rascher, U., Nedbal, L., 2006. Dynamics of photosynthesis in fluctuating light. Current Opinion in Plant Biology 9, 671–678.

Robertson, I., Li, L., Sherwin, S., Bearman, P., 2003. A numerical study of rotational and transverse galloping rectangular bodies. Journal of Fluids and Structures 17, 681–699.

Roden, J.S., 2003. Modeling the light interception and carbon gain of individual fluttering aspen (populus tremuloides michx) leaves. Trees—Structure and Function 17, 117–126.

Roden, J.S., Pearcy, R.W., 1993. Effect of leaf flutter on the light environment of poplars. Oecologia 93, 201–207.

Rodriguez, M., de Langre, E., Moulia, B., 2008. A scaling law for the effects of architecture and allometry on tree vibration modes suggests a biological tuning to modal compartmentalization. American Journal of Botany 95, 1523–1537.

Rodriguez, M., Ploquin, S., Moulia, B., de Langre, E., 2012. The multimodal dynamics of a walnut tree: experiments and models. Journal of Applied Mechanics 79, 4505.

Schuepp, P., 1972. Studies of forced-convection heat and mass transfer of fluttering realistic leaf models. Boundary-Layer Meteorology 2, 263–274.

Sellier, D., Fourcaud, T., 2005. A mechanical analysis of the relationship between free oscillations of pinus pinaster ait. Saplings and their aerial architecture. Journal of Experimental Botany 56, 1563–1573.

Tadrist, L., Saudreau, M., de Langre, E., 2014. Wind and gravity mechanical effects on leaf inclination angles. Journal of Theoretical Biology 341, 9–16.

Vogel, S., 1989. Drag and reconfiguration of broad leaves in high winds. Journal of Experimental Botany 40, 941–948.

Wick, B.H., 1954. Study of the subsonic forces and moments on an inclined plate of infinite span. Technical Report. Ames Aeronautical Laboratory.

Yamazaki, K., 2011. Gone with the wind: trembling leaves may deter herbivory. Biological Journal of the Linnean Society 104, 738–747.